Research Paper

Back-analysis of soil parameters of the Malutang II concrete face rockfill dam using parallel mutation particle swarm optimization

Yufeng Jia, Shichun Chi *

The State Key Laboratory of Coastal and Offshore Engineering, Dalian University of Technology, Dalian 116024, China
Institute of Earthquake Engineering, Dalian University of Technology, Dalian 116024, China

A R T I C L E I N F O

A B S T R A C T

Deformation control is a central problem in earth-rockfill dam design. The finite element method (FEM) is the primary method used to analyze and predict the deformation of earth-rockfill dams. The parameters of the constitutive model of soil used in earth-rockfill dams determine the FEM analysis results. Using prototype monitoring displacements, the soil parameters of the Malutang II concrete face rockfill dam were back-analyzed using parallel mutation particle swarm optimization. The calculated displacements of the back-analyzed soil parameters are consistent with the prototype monitoring results. The parallel mutation particle swarm optimization has a high optimization rate and can be used in large-scale practical engineering applications. The back-analysis results indicate that the deformation moduli of rockfills in the Malutang II are affected by construction situ.

1. Introduction

Deformation control is a central problem in earth-rockfill dam design. The accuracy of deformation control affects the deformation coordination among all areas in the dam body. Discordant deformation of a concrete face rockfill dam (CFRD) will cause the concrete slab to separate and break off from the cushion layer. Discordant deformation of a core wall rockfill dam will aggravate the core wall arching effect and will cause the clay core wall to break, which can even cause the dam body to failure. Furthermore, discordant deformation also affects the stress distribution in the dam body, which also influences the soil dynamic characteristics [1–3] and dam earthquake response.

The finite element method (FEM) is the primary method used to analyze and predict the deformation of earth-rockfill dams. The parameters of the constitutive model of soils used in dams determine the FEM analysis results. These parameters are usually measured in the laboratory using the triaxial compression tests and the maximum particle sizes in the samples are less than 60 mm. However, the maximum particle sizes of soils in earth-rockfill dams may be as large as 1 m. The particle size affects the deformation properties of gravelly materials [4]. The rockfill shear deformation modulus increases as the particle sizes become larger for a given sample diameter and increases with the sample diameter for a

given particle gradation [5,6]. Furthermore, in situ soil compaction differs from that observed in laboratories. In laboratory tests, the mass of the samples is accurately measured for each particle size group. The gradation, dry density, compaction degree, and porosity of the samples are well controlled. In situ soil compaction is controlled by compaction operation parameters and randomly sampled in situ tests. The compaction operation parameters, such as the number of compaction passes, the pavement or lift thickness, the roller velocity, and the excitation force, must be monitored and compared with compaction quality standards during the entire compaction operation. After compaction, soil samples are randomly selected from the compaction area. The gradation, dry density, compaction degree, and porosity of these samples are examined and compared with the design values. However, the use of a limited number of spot samples to represent the construction quality of the entire work area can be unreliable and sometimes misleading [7]. The compaction operation parameters are strongly affected by the engineers, supervisors and extensive management, making it difficult to ensure the compaction quality [8,9]. Hence, the resulting soil density and structure in the dam differ from those of laboratory samples. Finally, the rockfill used in situ is produced by quarry blasting. The particles contain many cracks, which can cause considerable particle breakage if they experience high stress. Particle breakage modifies the soil skeleton structures and affects the deformation characteristics. However, the smaller particles in the laboratory contain fewer cracks and generate less particle breakage. Thus, the parameters of a constitutive model that are determined in the laboratory may differ from those in situ.

---

* Corresponding author at: The State Key Laboratory of Coastal and Offshore Engineering, Dalian University of Technology, Dalian 116024, China.

Displacement back-analysis is an effective method for verifying and modifying soil parameters. Back-analyzed soil parameters can be used in deformation and stress analyses of earth-rockfill dams during construction and operation, which are beneficial to earth-rockfill dam safety operation, seismic safety assessment, and enforcement design.

Because the mechanical properties involved are complex, soil constitutive models are strongly nonlinear. It is difficult to directly calculate the soil parameters by inverting the earth-rockfill dam FEM displacement calculation. Thus, displacement back-analysis is applied by optimizing the soil parameters. The deviation between the calculated earth-rockfill dam displacements and the prototype monitoring values becomes an objective function. The optimal values of the soil parameters to be determined are progressively approximated through iteration by minimizing the fitness values of the objective function. During the soil parameter optimization, time-consuming FEM calculations are frequently performed; thus, the rate of convergence is slow, and the back-analysis fails for larger-scale problems.

In recent years, several more effective back-analysis methods have been developed. These methods primarily achieved improved back-analysis effectiveness by using intelligent optimization algorithms and intelligent computing techniques or a combination thereof. Intelligent optimization algorithms can accelerate the soil parameter optimization and thus avoid unnecessary fitness value calculations [10–16]. Intelligent computing techniques calculate the fitness values faster than the FEM [17,18]. However, the results of intelligent optimization algorithms are affected by the initial parameter values, and a local minimum or premature convergence is often obtained [17]. Intelligent computing techniques also require many FEM calculations for training, which consume a considerable amount of time. Furthermore, the results of intelligent computing techniques are affected by the training process, and the solution is sometimes unstable. Recently, a parallel algorithm was used in geotechnical engineering back-analyses [19–21].

These parallel algorithm back-analysis methods use intelligent optimization algorithms to optimize the parameters and accelerate the fitness value calculations using a parallel FEM with a multi-core central processing unit (CPU). The parallel FEM operates at two different levels. One of the parallel FEM levels simultaneously calculates the fitness values of the multi-group parameters using multiple cores. The other parallel FEM level calculates the fitness values of one group of parameters with multiple cores. The former has a higher effectiveness and a simpler program structure than the latter. The latter can perform larger-scale calculations, but its program structure is complicated, with lower calculation effectiveness in comparison to the former.

The Malutang II CFRD was built in 2009. The displacements measured in situ for this dam differ greatly from the values calculated using the FEM with soil parameters determined by a laboratory triaxial test. Thus, these soil parameters cannot be used to establish a reliable deformation and stress state of the dam to monitor the operation and to analyze the seismic safety.

In this paper, the soil parameters of the Malutang II CFRD were back-analyzed using an intelligent parallel algorithm back-analysis method, in which the soil parameters are optimized by mutation particle swarm optimization (MPSO) and the fitness values of the particle swarm are calculated using a parallel FEM.

2. Malutang II CFRD

The Malutang II CFRD is located along the Panlong River in the Yunnan province of China (Fig. 1). Along the crest, the dam is 154 m high and 493.4 m long; the upstream dam slope is 1:1.4, and the downstream integrated dam slope is 1:1.3. The storage capacity is $5.36 \times 10^8 \, m^3$, and the installed capacity of electric power plant is 300 MW. A typical section of this dam is shown in Fig. 2. Fig. 2 shows that the dam materials include main rockfill, secondary rockfill, transition, cushion, weighted cover and concrete face slab.

3. Displacement monitoring system

A detailed settlement monitoring system was established to monitor the deformation of the Malutang II CFRD [22]. Vertical displacements in the dam body were measured using settlement gauges distributed throughout typical cross-sections at 0 + 233.159. Twenty-two hydraulic overflow settlement gauges along three monitoring lines were placed in typical sections, of which 19 survived (at elevations of 522, 556, and 590 m). Two other monitoring gauges assessing the settlement and horizontal displacement were distributed on the downstream slope of typical sections at elevations of 565 and 595 m. The layout of the displacement gauges in typical section is presented in Fig. 3; the gauge positions are listed in Table 1.
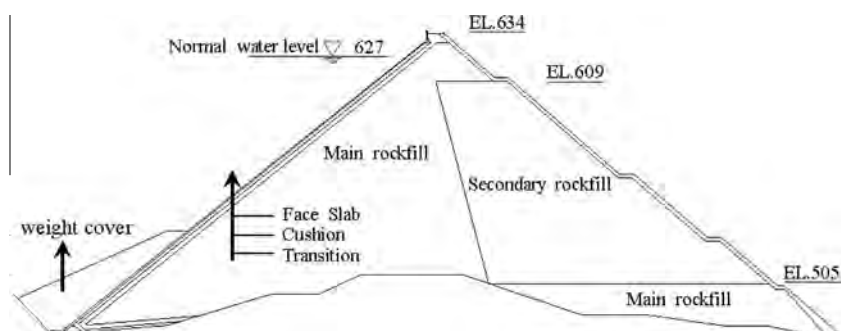

Fig. 1. General view of the Malutang II CFRD.

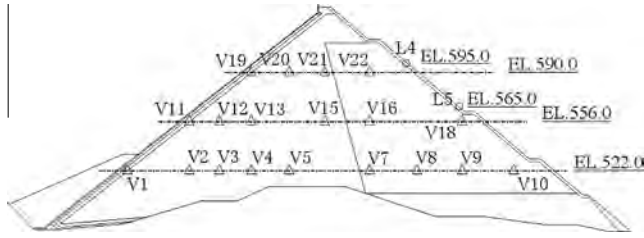Fig. 2. Typical section of the Malutang II CFRD at 0 + 233.159.

Fig. 3. Layout of the monitoring gauges in the 0 + 233.159 section of the Malutang II CFRD.

4. Objective function of the back-analysis

The fitness value of the objective function is the basis of the back-analysis. According to displacements of dam body, the objective function is developed, which is expressed as followed

$$F(y) = \sum_{i=1}^{in} \frac{1}{im} \sum_{j=1}^{im} \left(\frac{y_{ij}^c}{y_{ij}^s} - 1.0 \right)^2 \tag{1}$$

where $F(y)$ is the fitness value, in is the number of monitoring lines, im is the number of monitoring gauge displacements in one monitoring line, and y_{ij}^c and y_{ij}^s are the calculated displacement and the prototype monitoring displacement, respectively, at the j-th displacement in the i-th monitoring line. The settlements in the middle area of the dam are much larger than the settlements at the bottom and the top of the dam. Thus, the term $\frac{y_{ij}^c}{y_{ij}^s}$ in Eq. (1) minimizes the magnitude error of the displacements measured in situ. Fig. 3 shows that there are more monitoring gauges at EL.522m than at the other two monitoring lines. The $\frac{1}{im}$ term in Eq. (1) eliminates the gauge number difference among the monitoring lines. The weight of the each monitoring gauge displacement in every monitoring line is the same.

4.1. Displacement calculation

The displacement of Malutang II was calculated using the FEM. To calculate the displacement, Duncan and Chang's E–B model was used to simulate the stress–strain characteristics of the soil [23].

4.1.1. Constitutive model and soil parameters

The Duncan and Chang's E–B model is a simple and practical nonlinear elastic model. It is recommended by Chinese *Design specification for rolled earth-rockfill dams* (DL-5395-2007) to calculate displacement and stress of earth-rockfill dam. The Chinese *Specification of soil test* (SL237-1999) also provides techniques, which are used to determine soil parameters used in the Duncan and Chang's E–B model according to triaxial test results. The Chinese engineering practices indicate that the Duncan and Chang's E–B model can well simulate the settlements of earth-rockfill dams, whose computational accuracy satisfies the demand for engineering. However, many new constitutive models have been developed, which are

more sophisticated than the Duncan and Chang's E–B model. But the parameters of these constitutive models are difficult to determine and these constitutive models are also complex to use.

The Duncan and Chang's E–B model had been used to calculate displacement and stress of the Malutang II CFRD in the design processes. The model suggested that the tangent modulus E_t is expressed as follows:

$$\begin{cases} E_t = (1 - R_f S)^2 \cdot K \cdot P_a \cdot (\sigma_3/P_a)^n \\ S = \dfrac{(1 - \sin\phi)(\sigma_1 - \sigma_3)}{2c\cos\phi + 2\sigma_3\sin\phi} \end{cases} \tag{2}$$

where R_f is the failure ratio, S is the stress level, K is the modulus number, P_a is the atmospheric pressure equal to 101.3 kPa, σ_3 is the minor principal stress, n is the modulus exponent, σ_1 is the major principal stress, ϕ is the friction angle, and c is the cohesion.

The nonlinear volume change is simulated using the bulk modulus, which is expressed as follows:

$$B = K_b \cdot P_a \cdot (\sigma_3/P_a)^m \tag{3}$$

where K_b is the bulk modulus number and m is the bulk modulus exponent.

Under unloading and reloading conditions, the tangent modulus E_t is replaced by the unloading–reloading modulus E_{ur}, which is expressed as

$$E_{ur} = K_{ur} \cdot P_a \cdot (\sigma_3/P_a)^n \tag{4}$$

where K_{ur} is the unloading–reloading modulus number. The ratio K_{ur}/K varies from approximately 1.2 for stiff soils, such as dense sand, to approximately 3 for softer soils, such as loose sand [23].

The unloading and reloading conditions are determined using the loading function, which is expressed as

$$S_s = S \sqrt[4]{\sigma_3/P_a} \tag{5}$$

The maximum S_s of the soil during loading is denoted by S_{sm}. If $S_s > S_{sm}$, the soil is under loading conditions, and the tangent modulus E_t is used. If $S_s < 0.75 S_{sm}$, the soil is under unloading and reloading conditions, and the unloading–reloading modulus E_{ur} is used. If $S_{sm} > S_s > 0.75 S_{sm}$, the tangent modulus is determined using linear interpolation [24].

$$E_t' = E_t + (E_{ur} - E_t) \frac{S_s - 0.75 S_{sm}}{0.25 S_{sm}} \tag{6}$$

The Mohr–Coulomb envelopes for cohesionless soils are curved to some extent, and a wider range of pressure corresponds to a greater curvature, particularly for gravel and rockfill. For example, at the bottom near the center of a large dam, the rockfill may be confined under such a large pressure that the friction angle is

$$\phi = \phi_0 - \Delta\phi \cdot \log(\sigma_3/P_a) \tag{7}$$

where ϕ_0 is the value of ϕ for $\sigma_3 = P_a$, and $\Delta\phi$ is the reduction in ϕ for a 10-fold increase in σ_3 [23]. Thus, the friction angle ϕ and the cohesion stress c in Eq. (2) should be replaced by ϕ_0 and $\Delta\phi$, respectively, for rockfill materials.

There are eight parameters in Duncan and Chang's E–B model: K, n, K_{ur}, K_b, m, R_f, c, and ϕ (or ϕ_0 and $\Delta\phi$). The soil parameters used

Table 1
Positions of the monitoring gauges in the Malutang II CFRD.

Dam 0 + 233.159	Horizontal coordinate (m)										
Elevation (m)	−151	−104	−80	−56	−28	0	35	64.8	70	105	145
522	V1	V2	V3	V4	V5		V7		V8	V9	V10
556		V11	V12	V13		V15	V16			V18	
565										L5	
590				V19	V20	V21	V22				
595								L4			

in Duncan and Chang's E–B model for Malutang II were determined using a conventional consolidated-drained triaxial compression test. The stress–strain behavior during triaxial drained compression tests at different confining pressure values on the main rockfill is shown in Fig. 4. According to Duncan and Chang's E–B model suggestion, stress–strain curves in Fig. 4(a) can be approximated reasonably by hyperbolas

$$\sigma_1 - \sigma_3 = \varepsilon_1/(a + b\varepsilon_1) \tag{8}$$

where $a = 1/E_i$, E_i is the value of E_t when ε_1 equals 0; $b = 1/(\sigma_1 - \sigma_3)_{ult}$, $(\sigma_1 - \sigma_3)_{ult}$ is asymptotic value of $\sigma_1 - \sigma_3$ when ε_1 becomes infinity. The a or E_i and b or $(\sigma_1 - \sigma_3)_{ult}$ can be obtained using the stress–strain curves in Fig. 4(a) by Eq. (8).

$$R_f = \frac{(\sigma_1 - \sigma_3)_f}{(\sigma_1 - \sigma_3)_{ult}} \tag{9}$$

where $(\sigma_1 - \sigma_3)_f$ is a $\sigma_1 - \sigma_3$ at failure, which can be estimated from Fig. 4(a).The friction angle ϕ can be calculated by $\sin \phi = \frac{(\sigma_1 - \sigma_3)_f}{(\sigma_1 + \sigma_3)_f}$ for every σ_3, and then ϕ_0 and $\Delta\phi$ were determined according to relationship of $\phi \sim \sigma_3$, i.e., Eq. (7).

Fig. 5 shows the variation of initial tangent modulus E_i with σ_3, the values of K and n can be determined from this relationship $\lg(E_i/P_a)$–$\lg(\sigma_3/P_a)$.

The bulk modulus B_t is determined using the following function

$$B_t = \frac{\sigma_1 - \sigma_3}{3\varepsilon_v} \tag{10}$$

Fig. 6 shows the variation of bulk modulus B_t with σ_3, the values of K_b and m can be determined. And all the soil parameters determined using indoor triaxial tests are listed in Table 2.
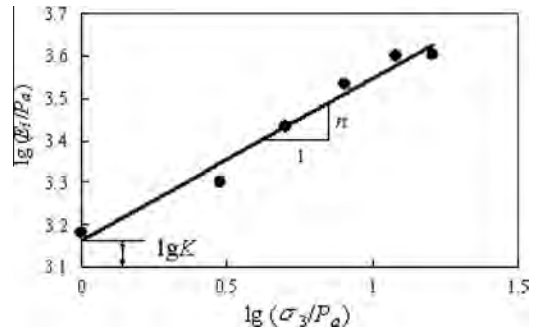

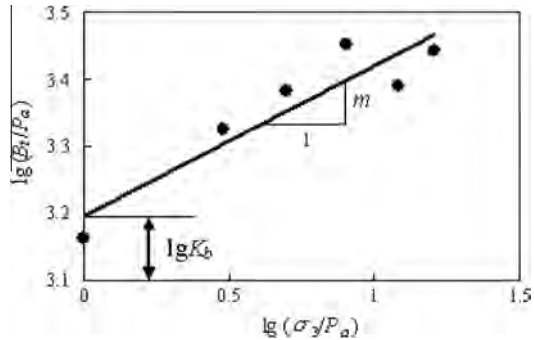**Fig. 5.** $\lg(E_i/P_a)$–$\lg(\sigma_3/P_a)$ curve.

Fig. 6. $\lg(B_t/P_a)$–$\lg(\sigma_3/P_a)$ curve.

Table 2
Duncan and Chang's E–B model parameters determined by a triaxial test.

Material	K	n	R_f	φ (°)	$\Delta\varphi$ (°)	K_b	m
Main rockfill	1467	0.38	0.80	55.0	15.0	1570	0.23
Secondary rockfill	1042	0.53	0.75	50.7	10.5	933	0.08
Cushion	1963	0.35	0.74	55.5	13.2	1742	0.21
Transition	1583	0.35	0.74	57.6	16.5	1590	0.16
Weighted cover	1042	0.53	0.75	50.7	10.5	933	0.08

Fig. 7. Three-dimensional FE mesh of Malutang II.

4.1.2. Finite element mesh and construction simulation

The three-dimensional finite element mesh of Malutang II is shown in Fig. 7; it is composed of 8284 elements.

The interface between the slab and the cushion was simulated using Goodman contact elements [25], which were also applied to simulate the slab joints and the peripheral joints. The shear modulus of the interface element, which was calculated using a hyperbolic model proposed by Clough and Duncan [26], is expressed as
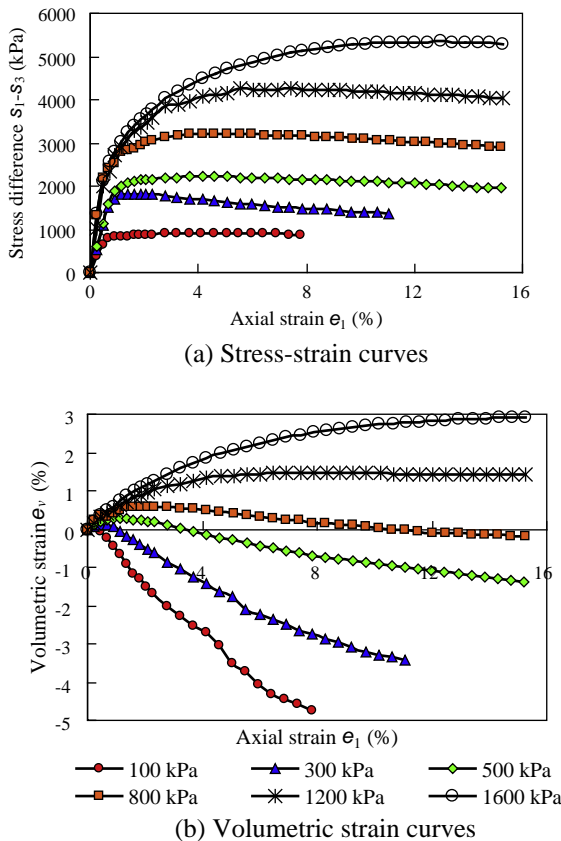

Fig. 4. Stress-axial strain-volumetric strain behaviors during triaxial drained compression tests at different confining pressure values on main rockfill.
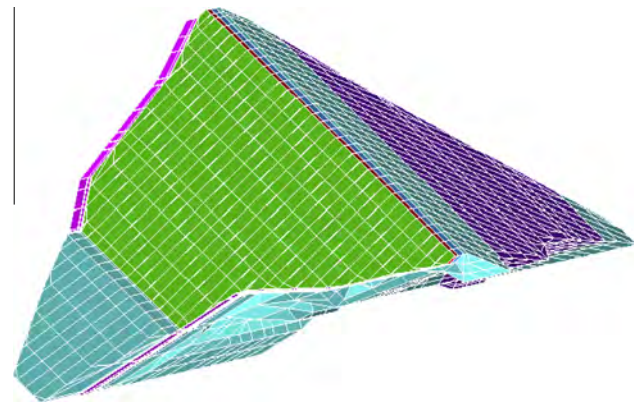
$$K_{yx} = K_1 \gamma_w \left(\frac{\sigma_y}{P_a}\right)^{n'} \left(1 - \frac{R_f' \tau_{yx}}{\sigma_y tg\delta}\right)^2$$

$$K_{yz} = K_1 \gamma_w \left(\frac{\sigma_y}{P_a}\right)^{n'} \left(1 - \frac{R_f' \tau_{yz}}{\sigma_y tg\delta}\right)^2 \quad (11)$$

where γ_w is the bulk density of water, K_{yx} and K_{yz} are the tangential coefficients of the shear modulus, σ_y is the normal stress, τ_{yx} and τ_{yz} are the shear stresses, and K_1, n', R_f', and δ are the modulus parameters. These parameters were determined from a direct shear test which conducted on an interface between the face slab and the cushion, where $K_1 = 4,500$, $n' = 0.5$, $\delta = 32°$, and $R_f' = 0.65$. The modules of the Goodman elements simulated the vertical joints between the face slabs using a water stop model [27]. The concrete face slab was simulated using a linear elastic model with an elastic modulus of 25.5 GPa and a Poisson ratio of 0.167.

The construction stages of the Malutang II dam are presented in Fig. 8. According to the stages shown in Fig. 8, the construction of Malutang II was simulated with 26 loading steps in the FEM calculation, in which step 1–3 simulated stage I, step 4–10 simulated stage II and stage I slab, step 11–19 simulated stage III, and step 20–26 simulated stage IV and stage II slab. In the construction, water was sprinkled adequately to ensure the rockfill was rolled more easily to design density. However, the pore water pressure of the rockfill did not rise because of the large permeability coefficient. This is in accord with drained triaxial test condition. The calculated displacements at the monitoring gauges until Mar.15th, 2009 are listed in Table 3. In Table 3, $L4_{horizontal}$ and $L5_{horizontal}$ are the horizontal displacements, and the others are the vertical settlements.

4.2. Prototype monitoring displacements

The displacements measured in situ are also listed in Table 3. These displacements represent the total values recorded until Mar.15th, 2009, immediately after the dam construction was
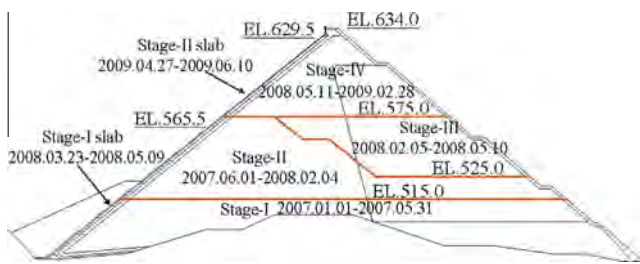
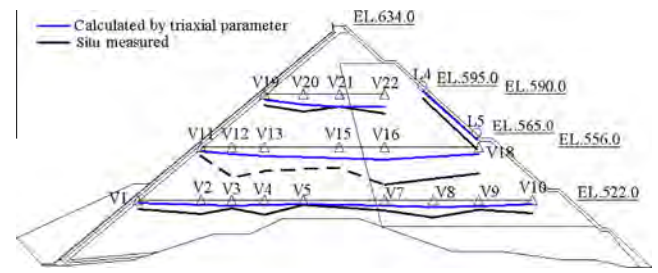**Fig. 8.** Construction stages of the Malutang II CFRD.

Fig. 9. Comparison of simulations based on triaxial test parameters and in situ measurements for settlements after construction (settlement amplified 20-fold).

completed, before the reservoir started impounding [28]. Furthermore, the displacements on L4 and L5 during construction are also recorded, which are shown in Fig. 16. The settlements measured in situ and the FEM-calculated values are shown in Fig. 9. The total number of measurements available for the back-analysis is 41.

The settlements from V11 to V15 were not recorded before the dam elevation reached 556 m in stage III due to in situ limitations [22]. Therefore, these settlements are italicized in Table 3 and denoted by a dashed line in Fig. 9. Hence, the settlements in construction stage II cannot be used to directly calculate the fitness values. These settlements can be used as a constraint of the back-analysis. If the sum of the calculated settlements from V11 to V15 was smaller than the in situ measurements, then the fitness values were set to infinity.

5. Parameter-searching range in back-analysis

Fig. 3 and Table 3 show that the observation points are primarily displaced by deformation of the main rockfill, the secondary rockfill, and the weight cover. Thus, the parameters of Duncan and Chang's E–B model for these rockfill materials were back-analyzed according to the prototype monitoring displacements.

Table 3 and Fig. 9 show that the displacements calculated according to the parameters determined by the indoor triaxial tests are smaller than the in situ measurements. The largest measured settlement is 119.6 cm at V16, whereas the simulated settlement based on the triaxial test parameters is only 40.9 cm. The horizontal displacements at L4 and L5 are 6.4 and 28.2 cm, respectively, whereas the calculated displacements are 15.9 and 23.0 cm, respectively. The simulated displacements differ significantly from the in situ monitoring results, even though the scale effect of the triaxial test and the limitations of Duncan and Chang's E–B model were eliminated.

Figs. 8 and 9 show that the calculated settlements and the in situ measurement values in stage III have the largest difference,

Table 3
Monitored and calculated displacements at the monitoring gauges.

Monitoring gauges	Displacement (cm)			Monitoring gauges	Displacement (cm)		
	Measured	Calculated			Measured	Calculated	
		Triaxial test	Back-analysis			Triaxial test	Back-analysis
V1	29.1	8.5	16.7	V15	63.6	35.4	102.8
V2	44.2	16.0	29.8	V16	119.6	40.9	106.9
V3	27.0	17.7	33.2	V18	84.6	22.9	60.1
V4	46.4	14.6	29.7	V19	36.4	18.8	40.3
V5	15.5	12.2	26.2	V20	56.4	32.7	67.3
V7	33.5	18.6	49.1	V21	40.8	40.7	79.9
V8	56.5	22.5	57.1	V22	63.3	39.8	72.7
V9	32.0	19.7	47.2	$L4_{vertical}$	37.9	20.5	38.7
V10	42.1	12.3	26.9	$L4_{horizontal}$	6.4	15.9	9.1
V11	26.4	13.3	33.1	$L5_{vertical}$	51.2	15.5	38.7
V12	99.2	21.5	55.3	$L5_{horizontal}$	28.2	23.0	26.2
V13	76.5	28.4	74.6				

Table 4
Parameter-searching range of Duncan and Chang's E–B model.

Material	K	n	R_f	φ (°)	$\Delta\varphi$ (°)	K_b	m
Main rockfill I	700–2200	0.15–0.40	0.60–0.90	45.0–55.0	5.0–16.0	300–1800	0.05–0.30
Main rockfill II	300–2200	0.15–0.45	0.60–0.90			300–1500	0.10–0.50
Main rockfill III	800–2200	0.15–0.45	0.60–0.90			500–1800	0.05–0.50
Secondary rockfill I	700–1500	0.20–0.60	0.60–0.90	40.0–50.0	5.0–16.0	300–1500	0.05–0.50
Secondary rockfill II	300–1500	0.15–0.60	0.60–0.90			200–1200	0.05–0.50
Secondary rockfill III	700–1500	0.15–0.60	0.60–0.90			300–1500	0.05–0.50

followed by the differences in stages I and IV. The monthly construction speed was 2.0×10^5 m^3 in stage I, 2.85×10^5 m^3 in stage II, and 2.47×10^5 m^3 in stages III and IV [29]. The measured displacements and the construction record indicate that the rapid construction reduced the consolidation time [29], modified the structure of the rockfill, and caused the rockfill density to be unevenly distributed. The uneven density of the rockfill affected the rockfill deformation modulus and the dam body displacement. According to the construction record, the main rockfill and the secondary rockfill were separated into three parts corresponding to the three construction rates. Thus, the main rockfill types I, II, and III represent the main rockfill types that are constructed in stages I, II, and III & IV, respectively. The same notation is applied for secondary rockfill. Fig. 8 and Table 2 show that the weighted cover material is identical to the secondary rockfill and was constructed in stage IV. Thus, the weighted cover rockfill material was also simulated using secondary rockfill II in the back-analysis.

Therefore, Duncan and Chang's E–B model parameters K, n, R_f, ϕ_0, $\Delta\phi$, K_b, and m of the main rockfill and the secondary rockfill in these construction periods were back-analyzed. The searching range of the parameters to be back-analyzed was determined according to experience and the results of the triaxial laboratory tests, as shown in Table 4. There are 34 parameters that must be back-analyzed. The unloading–reloading modulus number K_{ur} was set to 1.5 times K, as was done for the triaxial test parameters.

6. Parallel MPSO displacement back-analysis method

6.1. Mutation particle swarm optimization

Particle swarm optimization (PSO) is a population-based heuristic technique. This optimization is based on a simplified social model simulations, which are used to visualize the movements of a flock of birds or particles [30,31]. It is a simple and effective algorithm to optimize continuous nonlinear functions and is widely used in Geotechnical engineering [14,19,20]. In this algorithm, the potential solution of the parameter optimization is simulated using a particle location in a hyperspace. The solution is searched by a particle swarm flying in the hyperspace. The particles fly with a randomized velocity and change location. Based on the parameter optimization problem, the fitness values of each location are calculated. The best location achieved by each particle is called *pbest*. The best location achieved by the entire particle swarm is called *gbest*. Each particle updates its (accelerating) velocity according to its *pbest* and *gbest*. The acceleration is weighted by a random term, where separate random numbers are generated to accelerate toward *pbest* and *gbest* [30]. The particle location and velocity are expressed as

$$x_i(t+1) = x_i(t) + v_i(t+1) \tag{12}$$

$$v_i(t+1) = wv_i(t) + c_1r_1[p_i(t) - x_i(t)] + c_2r_2[p_g(t) - x_i(t)] \tag{13}$$

where t is an iteration counter, $x_i(t) = (x_{i1}, x_{i2}, \ldots, x_{ik})$ is the current location of the i-th particle in the swarm, k is the hyperspace dimension, $i = 1, 2, \ldots, j$, j is the particle number of the particle

swarm, $x_i(t+1)$ is the update location, $v_i(t) = (v_{i1}, v_{i2}, \ldots, v_{in})$ is the current velocity, $v_i(t+1)$ is the update velocity, w is an inertia weighting parameter, c_1 and c_2 are acceleration constants with positive real values, r_1 and r_2 are random numbers in (0,1), $p_i(t)$ is the *pbest* value of the i-th particle, and $p_g(t)$ is the *gbest* value of the entire particle swarm [30,31].

The results of traditional PSO are affected by the particles' initial values, and a local minimum or premature convergence is often obtained [17,32,33]. Thus, using a genetic algorithm, a nonlinear mutation was added after the particle acceleration. The mutation randomly generates mutational particles between the current location of the particle and the hyperspace boundary. If the mutational particle value is better than the *pbest* fitness values, the particle will replace *pbest*. The mutational-particle location is expressed as

$$x_i^m(t) = \begin{cases} x_i(t) + [u - x_i(t)] \cdot [1 - rand^{(1-t/T_{max})\cdot d}] & random(0,1) = 0 \\ x_i(t) + [x_i(t) - l] \cdot [1 - rand^{(1-t/T_{max})\cdot d}] & random(0,1) = 1 \end{cases} \tag{14}$$

where u is the hyperspace upper boundary, l is the hyperspace lower boundary, *rand* is a random number generated according to a uniform distribution in (0,1), T_{max} is the maximum iteration number, d is a system parameter equal to 2, and $random(0,1)$ is a random number equal to 0 or 1 [33].

6.2. Procedures of the MPSO displacement back-analysis

The searching ranges of the 34 soil parameters listed in Table 4 constituted a 34-dimensional searching space. A particle location $x_i(t) = (k_{i1}, n_{i2}, \ldots, m_{i34})$ in the 34-dimensional searching space is a group of 34 soil parameters. So in the MPSO displacement back-analysis, the back-analysis of the 34 soil parameter was changed to search a best location using the particle swarm in the 34-dimensional searching space. The procedure of the MPSO displacement back-analysis includes the following steps.

(1) Generate m particles with random locations in the 34-dimensional searching space. The m different particles, each of whose particle location has 34 soil parameters, constitute a particle swarm. Set the values of w, c_1, c_2, T_{max}, and Tolerance, and assign t to 0.

(2) Calculate displacements of the rockfill dam using the FEM according to a particle location $x_i(t) = (k_{i1}, n_{i2}, \ldots, m_{i34})$, which is consisted by the 34 soil parameters. According to the calculated displacements and the prototype monitoring displacements of the rockfill dam, calculate the fitness value of each particle location $x_i(t)$ using Eq. (1).

(3) According to these fitness values, the *pbest* and *gbest* of the particle swarm were determined. According to the *pbest* and *gbest*, the m particles were accelerated using Eqs. (12) and (13). The particle location $x_i(t)$ was updated to $x_i(t+1)$.

(4) Calculate displacements of the rockfill dam using the FEM according to an updated particle location $x_i(t+1) = (k_{i1}, n_{i2}, \ldots, m_{i34})$. According to the calculated displacements

and the prototype monitoring displacements, calculate the fitness value of each updated particle location $x_i(t+1)$ using Eq. (1).

(5) Replace *pbest* of each particle with the updated location $x_i(t+1)$ if the latter's fitness value is less than that of *pbest*. Replace *gbest* with *pbest* if the latter's fitness value is less than that of *gbest*.

(6) According to the update *pbest* and *gbest*, generate mutational particles $x_i^m(t) = (k_{i1}^m, n_{i2}^m, \ldots, m_{i34}^m)$ using Eq. (14).

(7) Calculate displacements of the rockfill dam using the FEM according to a mutational particle location $x_i^m(t)$. According to the calculated displacements and the prototype monitoring displacements, calculate the fitness value of each mutational particle using Eq. (1).

(8) Replace *pbest* and updated particle location of each particle with the mutational particle location $x_i^m(t)$ if the latter fitness value is less than *pbest*.

(9) Update t with $t+1$. Finish the optimization if t equals T_{max} or if the fitness value of *gbest* is less than Tolerance. Update w with $w_0-(w_0-0.01)\cdot t/T_{max}$ and return to procedure (3) if t is less than T_{max}.

The inertia weighting w affects the performance of the PSO. A higher w value will help in avoiding a local minimum, and a lower w will accelerate the convergence. A PSO with a linearly decreasing w can improve the effectiveness [34]. Hence, w is replaced by $w_0-(w_0-0.01)\cdot t/T_{max}$ in procedure (9), where w_0 is the initial value of w in procedure (1).

In the procedures of the MPSO displacement back-analysis, procedures (2), (4) and (7) calculate the fitness values of the particle swarm using the FEM. This process will be time-consuming if the fitness values of the particle swarm are calculated one by one with a serial calculation by one core. However, the fitness value calculations of each particle in each of these three procedures are completely independent. Therefore, the computation time can be reduced if the fitness values of multiple particles can be simultaneously calculated using a parallel FEM with multiple cores.

6.3. Parallel MPSO displacement back-analysis procedure

A parallel FEM was programmed in Fortran 90 using the Message Passing Interface (MPI). The MPI provides a set of interfaces that are designed to assist the library in constructing a virtual topology from the application's communication pattern and in supporting remapping (reordering) of the processes to the available cores to optimize performance [35]. Communication among the cores is achieved by sending and receiving messages among the corresponding processes. In this case, one process sends the particle locations to the other processes and receives the fitness values of the particles from the others. This process is the master process. The initial generation, acceleration, and mutation of the particles are achieved by the master process. The other processes are slave processes, which calculate the fitness values of the particles using the FEM. The communications between the master process and the slave processes are shown in Fig. 10. Parameter $k1$ in Fig. 10 indicates the number of slave processes.

The particle locations, which are sent by the master process, and the fitness values, which are sent by the slave process, occupy little internal memory. Thus, the communications among processes cost little time. The effectiveness of the entire parallel FEM calculation is determined by the FEM calculations of the slave processes. To avoid slave process idling, the particle number of the particle swarm is an integer multiple of $k1$. Furthermore, the master process sends different particle locations. The calculation in each slave process costs different amounts of time. Thus, according to the slave process numbers, the master process sends the particle
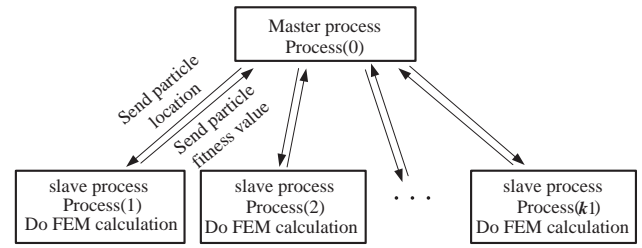

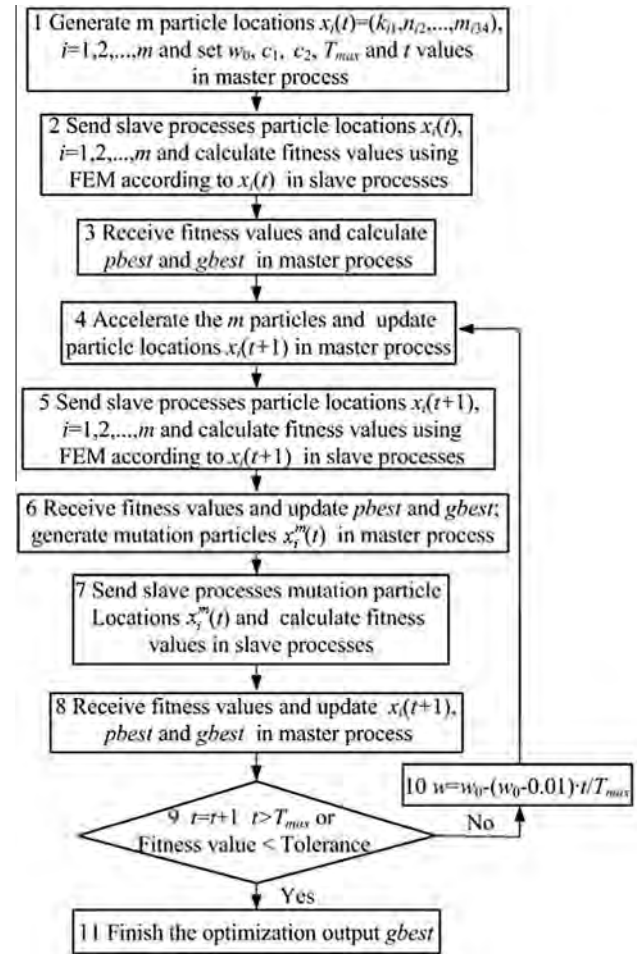
Fig. 10. Communication among processes.

**Fig. 11.** Flowchart of the parallel MPSO back-analysis.

locations in the first message-sending turn. The master process freely receives fitness values from the slave processes. In the following message-sending turn, the master process sends the slave processes a new particle location after its fitness value is received. This "first come first served" principle avoids slave process idling generated by the FEM calculation. A flowchart of the parallel MPSO back-analysis is shown in Fig. 11.

The reliability of MPSO is examined by two benchmark functions, Griewank and Rosebrock. The formula and searching range of benchmark functions are listed in Table 5. The benchmark functions in three dimensions are shown in Fig. 12. Fig. 12 shows that the Griewank is a multimodal test function, while the Rosenbrock is a unimodal function, whose global optimum locates in a narrow valley.
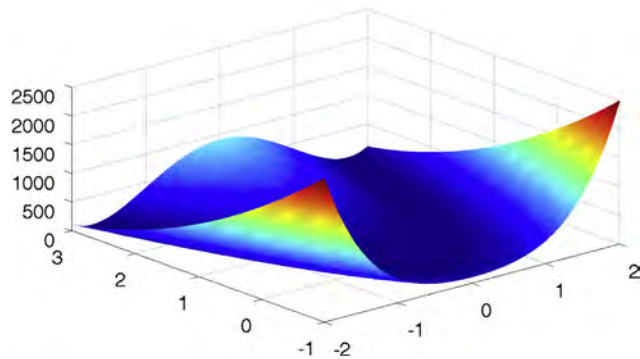
In the examination, the searching hyperspace dimension k, the particle swarm j, the initial inertia weighting w_0, the acceleration

Table 5
Benchmark functions and testing results.

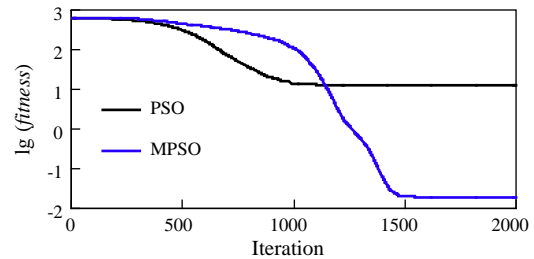| Name	Formula	Range	Average best fitness (Standard deviation)	
			PSO	MPSO
Griewank	$f_1(x) = \sum_{i=1}^{k} \frac{x_i^2}{4000} - \prod_{i=1}^{k} \cos(\frac{x_i}{\sqrt{i}}) + 1$	$[-600,600]$	1.27E+01(3.17E+01)	1.84E−02(1.80E−01)
Rosenbrock	$f_2(x) = \sum_{i=1}^{k-1}(100(x_{i-1} - x_i^2)^2 + (x_i - 1)^2)$	$[-30,30]$	1.89E+04(3.59E+04)	1.08E+02(8.98E+01)
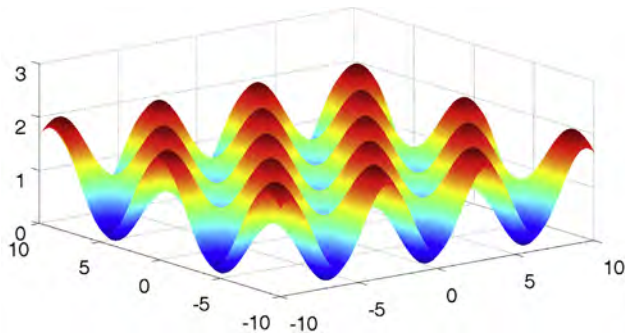
(a) Griewank (k=2)

(b) Rosenbrock (k=2)

Fig. 12. Benchmark functions.

(a) Average fitness of Griewank

(b) Average fitness of Rosenbrock

Fig. 13. Evolution of average fitness for PSO and MPSO.

Fig. 14. Time consumed by parallel calculations for one iteration.

constants c_1 and c_2, and the maximum iteration number T_{max} were set as 30, 30, 1.0, 2.0, 2.0 and 2000. Each benchmark function was respectively performed by 50 times using the PSO and MPSO. The average best fitness value and dispersion of the examination were also listed in Table. 5. Fig. 13 shows the evolution of the logarithmic average fitness values for the PSO and MPSO. The MPSO achieved better results on all the benchmark functions than the PSO. The mutation of MPSO keeps the diversity of particle swarm and mitigates premature convergence.
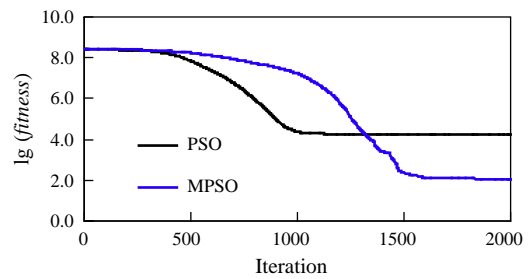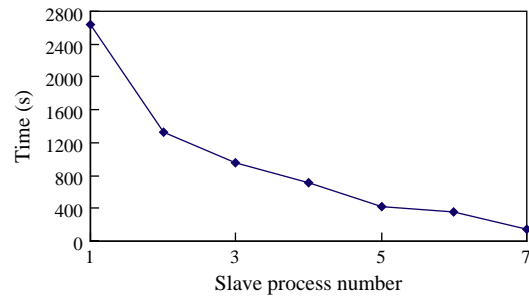
7. Parameters back-analysis

The rockfill parameters of Malutang II were back-analyzed using the parallel MPSO. The particle number of the particle swarm j, the initial inertia weighting w_0, the acceleration constants c_1 and c_2, the maximum iteration number T_{max}, and Tolerance were set as 22, 1.0, 2.0, 2.0, 1000, and 0.3, respectively.

The number of fitness value calculations performed by the FEM was $22 \times 1000 \times 2 = 44{,}000$. Seven slave processes were used to calculate the fitness values of the particle swarm. Four processes (equipped with a 3.41-GHz core) calculated the fitness value twice as fast as the others (equipped with a 2.33-GHz core). Hence, these 7 slave processes can perform 11 fitness value calculations as the 3 slower processes complete one. The particle swarm fitness value calculation required approximately 146 s for one iteration.

Fig. 14 shows the relationship between the slave process number and the fitness value calculation time of the particle swarm for one iteration. The fitness value calculation time decreased as the number of slave processes in the parallel calculation increased. The results of the back-analysis are shown in Table 6.

The FEM analysis was conducted using model parameters obtained from the back-analysis. The displacements calculated from the back-analysis parameters are listed in Table 3 in comparison with the in situ measurements and the calculated displacements based on triaxial test parameters. The fitness value of the calculated displacements for the triaxial test parameters was 1.162, while the value of the back-analysis parameters was 0.398. The calculated and the in situ measured settlements until Mar. 15th, 2009 are shown in Fig. 15. The calculated and the in situ measured displacements on L4 and L5 during construction are shown in Fig. 16. Fig. 16 shows that the displacements increase

Table 6
Duncan and Chang's E–B model parameters from the back-analysis.

| Methodology	Material	K	n	R_f	φ (°)	$\Delta\varphi$ (°)	K_b	m
Triaxial test	Main rockfill	1467	0.38	0.80	55.0	15.0	1,570	0.23
	Secondary rockfill	1042	0.53	0.75	50.7	10.5	933	0.08
Back-analysis	Main rockfill I	1011	0.33	0.90	55.0	16.0	1112	0.22
	Main rockfill II	712	0.40	0.85			422	0.45
	Main rockfill III	1545	0.18	0.60			1663	0.47
	Secondary rockfill I	901	0.22	0.62	50.0	5.0	517	0.15
	Secondary rockfill II	311	0.20	0.90			207	0.05
	Secondary rockfill III	1200	0.31	0.60			558	0.32
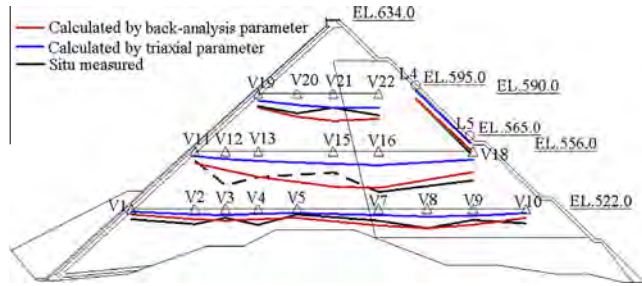
Fig. 15. Comparison of simulations and in situ measurements for settlements after construction (settlement amplified 20-fold).

with construction elevation. In the back-analysis, the $\frac{y_{ij}^c}{y_{ij}^s}$ on L4 and L5 were calculated according to the following function:

$$\frac{y_{ij}^c}{y_{ij}^s} = \frac{1}{n_L} \sum_{l=1}^{n_L} \frac{y_{ij,l}^c}{y_{ij,l}^s} \qquad (15)$$

where n_L is the number of loading steps, $y_{ij,l}^c$ and $y_{ij,l}^s$ are the calculated displacement and the prototype monitoring displacement in the l-th loading step, respectively.

The settlements calculated using the back-analysis parameters are consistent in magnitude and distribution with the values measured in situ. Therefore, in general, the back-analysis results satisfactorily reflect the deformation properties of the dam.

Table 6 shows a comparison between the triaxial test parameters and the back-analysis parameters of the main rockfill and the secondary rockfill, respectively. The back-analyzed values of K and K_b are less than the triaxial test values, except for K and K_b in main rockfill III and K in secondary rockfill III. The back-analyzed K and K_b of main rockfill III are the largest, and those of main rockfill I are larger than those of main rockfill II. Accordingly, main rockfill II has a higher construction speed than main rockfill III and main rockfill I, indicating that the construction speed significantly affects the deformation modulus of the main rockfill. This tendency is consistent with the distribution of the settlements measured in situ and the construction record [29]. Furthermore, the stress history of main rockfill II is different from main rockfill I and main rockfill II, which also affects its deformation modulus. The back-analyzed K and K_b of the secondary rockfill also followed this trend. Therefore, the settlements of V16, V18, and L5 are primarily generated by secondary rockfill II. The soft secondary rockfill II deformation below 525 m accounted for approximately 40% of the total settlement of these three points. The harder secondary rockfill III deformation between 525 m and 565 m accounted for approximately 30%. The secondary rockfill I and the main rockfill I deformation below 515 m accounted for approximately 30%. This result is consistent with the distribution of the settlements measured in situ [22,29]. The back-analyzed results indicate that construction speed and stress history affect the deformation modulus and the displacement of the dam body.
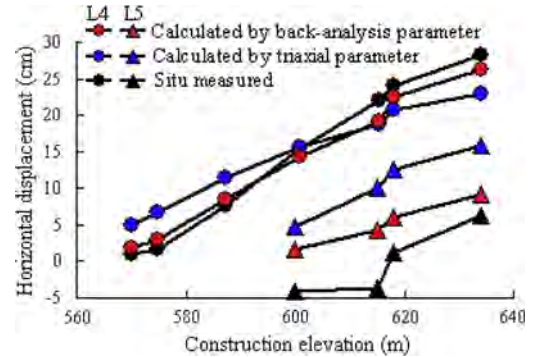
(a) Horizontal displacements
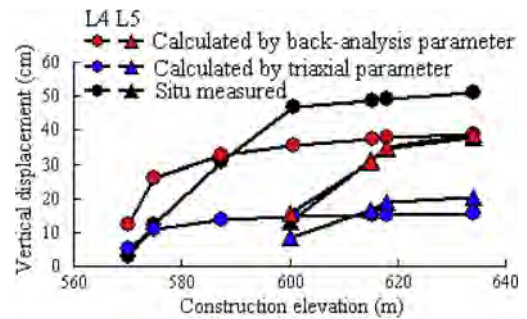
(b) Vertical displacements

Fig. 16. Displacements of simulations and in situ measurements on the L4 and L5 during construction.

8. Conclusion

The E-B model parameters of rockfill in the Malutang II CFRD were back-analyzed using a parallel MPSO. The displacements calculated from the back-analyzed parameters are consistent with the prototype monitoring results. The back-analyzed parameters can accurately describe the deformation characters of rockfill for use in safety operation, seismic safety assessment, and enforcement design. The parallel MPSO has a high optimization rate and can be used in large-scale practical engineering applications.

The back-analysis results indicate that the deformation moduli of rockfills in the Malutang II CFRD are affected by construction in situ, which should be considered in the back-analysis.

References

[1] Seed H Bolton, Wong Robert T, Idriss IM, Tokimatsu K. MODULI AND DAMPING FACTORS FOR DYNAMIC ANALYSES OF COHESIONLESS SOILS. J Geotechnical Eng 1986;112(11):1016–32.

[2] Eiichi Taniguchi, Whitman Robert V, Marr W Allen. PREDICTION OF EARTHQUAKE-INDUCED DEFORMATION OF EARTH DAMS. Soils Found 1983;23(4):126–32.

[3] Seed H Bolton, Martin Philippe P, Lysmer John. PORE-WATER PRESSURE CHANGES DURING SOIL LIQUEFACTION. Am Soc Civil Eng J Geotechnical Eng Div 1976;102(4):323–46.

[4] Donaghe Robert T, Cohen Melvin W. STRENGTH AND DEFORMATION PROPERTIES OF ROCK FILL[R]. S-78-1, U.S. Army Engineer Waterways Experiment Station, January, 1978.

[5] Chong LI, Chang-rong HE, Chen Wang, et al. Study of scale effect of large-scale triaxial test of coarse-grained materials. Rock Soil Mechan 2008:563–6.

[6] Junjie Hua, Wei Zhou, Xiaolin Chang, et al. Study of scale effect on stress and deformation of rockfill. Yanshilixue Yu Gongcheng Xuebao/Chinese J Rock Mechan Eng 2010;29(2):328–35.

[7] Liu Donghai, Sun Jing, Zhong Denghua, et al. Compaction quality control of earth-rock dam construction using real-time field operation data. J Construct Eng Manage ASCE 2012;138(9):1085–94.

[8] Denghua Zhong, Donghai Liu, Bo Cui. Real-time compaction quality monitoring of high core rockfill dam. Sci China Technol Sci 2011;54(7):1906–13.

[9] Dong-Hai Liu, Qian Wang, Bo Cui, et al. Control standards for compaction parameters of earth-rock dams under continuous construction process monitoring. Yantu Gongcheng Xuebao/Chinese J Geotechnical Eng 2013;35(9):1712–6.

[10] Ming-Jun Tian, Jing Zhou. Inversing soil mechanical parameters of embankment dam using ant colony algorithm. Yanshilixue Yu Gongcheng Xuebao/Chinese J Rock Mechan Eng 2005;24(8):1411–6.

[11] Zhi-Yu Song, Jun-Jie Li, Hong-Yu Wang. Inverse research for gravity dam parameters based on chaos artificial fish swarm algorithm. Yantu Lixue/Rock Soil Mech 2007;28(10):2193–6.

[12] She-Rong Zhang, Hui He. Application of improved genetic algorithm to back analyzing parameters of rockfill. Yantu Lixue/Rock Soil Mech 2005;26(2):182–6.

[13] Fei Kang, Li Jun-Jie, Qing Xu. Hybrid simplex artificial bee colony algorithm and its application in material dynamic parameter back analysis of concrete dams. Shuili Xuebao/J Hydraulic Eng 2009;40(6):736–42.

[14] Jia Shan-Po, Wu Guo-Jun, Chen Wei-Zhong. Application of finite element inverse model based on improved particle swarm optimization and mixed penalty function. Yantu Lixue/Rock Soil Mechan 2011;32(SUPPL.2):598–603.

[15] Hashash Youssef MA, Levasseur Severine, Osouli Abdolreza, et al. Comparison of two inverse analysis techniques for learning deep excavation response. Comput Geotechn 2010;37(3):323–33.

[16] Rechea C, Levasseur S, Finno R. Inverse analysis techniques for parameter identification in simulation of excavation support systems. Comput Geotech 2008;35(3):331–45.

[17] Yuzhen Yu, Bingyin Zhang, Huina Yuan. An intelligent displacement back-analysis method for earth-rockfill dams. Comput Geotech 2007;34(6):423–34.

[18] Dongjian Zheng, Lin Cheng, Tengfei Bao, et al. Integrated parameter inversion analysis method of a CFRD based on multi-output support vector machines and the clonal selection algorithm. Comput Geotech 2013;47:68–77.

[19] Bingrui Chen, Xiating Feng, Shuling Huang, et al. Inversion of viscoelasto-plastic parameters based on fast Lagrangian analysis of continuum-parallel particle swarm algorithm and its application. Yanshilixue Yu Gongcheng Xuebao/Chinese J Rock Mechan Eng 2007;26(12):2517–25.

[20] Zhang Xiaofei, Huai Xianfeng, Li Shouyi, et al. Back analysis of thermal parameters of roller compacted concrete dam based on parallel particle swarm optimization Piscataway. NJ (USA): IEEE; 2011.

[21] Shaohu Ni, Ming Xiao, Shihai He, et al. Back analysis in underground engineering based on parallel computing and optimization algorithm and its verification. Yanshilixue Yu Gongcheng Xuebao/Chinese J Rock Mechan Eng 2013;32(3):501–11.

[22] Jianying Wang, Dewu Huang. The displacement monitoring design and analysis of Malutang II CFRD. Yunnan Water Power 2011;05:28–31.

[23] Duncan JM, Byrne Peter, Wong Kai S, et al. Strength, stress-strain and bulk modulus parameters for finite element analyses of stresses and movements in soil masses. [R]. Berkeley: Univ of California: Report No. UCB/GT/80-011980

[24] Duncan JM. FEADAM 84: a computer program for finite element analysis of dams [DB/CD]. 1984.

[25] Goodman RE, Taylor RL, Brekke. A model for the mechanics of jointed rock. J Soil Mechan Found Div, ASCE 1968;94(SM3):637–59.

[26] Clough GW, Duncan JM. Finite element analysis of retaining wall behavior. J Soil Mech Found Eng 1971;97(12):1657–72.

[27] Ganchen Gu, Shen Changsong, Cen Weijun. Earthquake engineering for Earthrock dams. Beijing: China Water Power Press; 2009.

[28] Zhenhua Jia, Yongqing Chen, Shiqian Hui, et al. The review of the Malutang CFRD construction. Yunnan Water Power 2010;03:1–4.

[29] Wei Ma, Renjie Deng. Estimation of the Malutang II rapid construction. Yunan Water Power 2010;03:122–4.

[30] Eberhart R, Kennedy J. A new optimizer using particle swarm theory New York. NY (USA): IEEE; 1995.

[31] James Kennedy, Russell Eberhart. Particle swarm optimization Perth. Aust: IEEE; 1995.

[32] Parno MD, Hemker T, Fowler KR. Applicability of surrogates to improve efficiency of particle swarm optimization for simulation-based problems. Eng Optim 2012;44(5):521–35.

[33] Li Liang. Application of intelligent optimization algorithms to the soil slope stability analysis[D]. Dalian: Dalian University of Technology; 2005.

[34] Eberhart RC, Shi Y. Comparing inertia weights and constriction factors in particle swarm optimization California. CA (United states): IEEE; 2000.

[35] Rashti MJ, Green J, Balaji P, et al. Multi-core and network aware MPI topology functions Berlin. Germany: Springer Verlag; 2011.